Dynamic CuII/CuI speciation in Cu-CHA catalysts by in situ Diffuse Reflectance UV–vis-NIR spectroscopy

Dynamic Cu^{II}/Cu^{I} speciation in Cu-CHA catalysts by in situ Diffuse Reflectance UV-Vis-NIR spectroscopy

Chiara Negri[a], Matteo Signorile[a], Natale Porcaro[a], Elisa Borfecchia[a], Gloria Berlier[a]*, Ton V.W. Janssens[b] and Silvia Bordiga[a]*

[a] Department of Chemistry, NIS Centre of Excellence and INSTM Reference Center, University

of Turin, Via P. Giuria 7, 10125 10 Torino, Italy

[b] Umicore Denmark ApS, Nøjsomhedsvej 20, 2800 Kgs. Lyngby, Denmark

Abstract

Copper exchanged CHA were investigated by *in situ* Diffuse Reflectance UV-Vis-NIR spectroscopy in order to study the evolution of the copper environment in respect to the sample composition (2 samples differing in Si/Al and Cu content) and the activation procedure (in O_2 or N_2 from room temperature to 400 °C). *In situ* measurements allowed showing the different behavior of the two samples, both in the *d-d* and Ligand to Metal Charge Transfer regions, confirming a strong effect of the lattice composition to determine the copper environment and its reactivity. One of the two sample (Si/Al=15 and Cu/Al =0.5) was further investigated, in order to clarify the nature of the Cu-oxo species, formed along activation in oxygen. To shed light on this point, *in situ* measurements starting from a reduced form of the sample, obtained by activation in inert atmosphere at high temperature, were also considered. Additional suggestions on the nature of these species were obtained by resonant Raman measurements conducted in controlled atmosphere.

*Corresponding authors: gloria.berlier@unito.it, silvia.bordiga@unito.it

1. Introduction

Cu-CHA catalysts are obtained by ion exchange of chabazite (CHA), a small pore framework zeolite. These have been increasingly studied over the last decade, in relation to their activity (good performances in the 200-550 °C range and high thermal stability) for the Selective Catalytic Reduction of NO_x with NH_3 (NH_3-SCR) [1-5]. Many studies have been thus focused on the nature and location of Cu^{II} and Cu^{I} sites in the CHA cage, depending on the activation conditions and presence of reactants [6-11]. Most authors agree on the fact that after thermal treatments in oxidizing conditions Cu^{II} ions are present as a mixture of $Z[Cu^{II}(OH)]$ and Z_2Cu^{II}, where Z represents a negative charge delocalized on the framework oxygen atoms in the presence of one Al heteroatom. The former requires 1Al exchange sites for charge balance, while 2Al ones are needed to stabilize the latter, which are thus favored at low Si/Al ratio.

The relative stability of the different sites in the 6- or 8-membered rings of CHA frameworks (6MR or 8MR) has been widely discussed in the literature [8, 9, 11, 12]. Recent DFT and Molecular Dynamics simulations by Li et al. suggested that monomeric $Z[Cu^{II}(OH)]$ sites are energetically more favorable when oriented in the 8MR, while Z_2Cu^{II} can be found in two distinct structural arrangements in 6MR, involving framework Al atoms in 'meta' or 'para' positions [13]. Also, it was proposed that Cu^{II} ions first populate 2Al exchange sites, before populating remaining 1Al sites as $Z[Cu^{II}(OH)]$ [14]. Importantly, Al distribution in the CHA framework (and consequent Cu speciation) have been shown to be dependent on the synthesis conditions [15]. Namely, the presence of Na^+ ions during CHA synthesis causes a random Al distribution, so that the statistical analysis proposed by Paolucci et al. can be used to quantify the relative amount of $Z[Cu^{II}(OH)]$ and Z_2Cu^{II} [14]. On the other hand, N,N,N-trimethyl-1-adamantammonium cations ($TMAda^+$, used as structure directing agent for CHA synthesis) directs the formation of isolated Al framework atoms in the absence of Na^+ ions in the synthesis batch [15].

Bi-coordinated Cu^{I} ions (which can be located in both 6MR and 8MR) [11, 16] are formed during activation in inert conditions, through the so-called self-reduction, which is believed to involve only the $Z[Cu^{II}(OH)]$ ions. Moreover, a recent study based on advanced multivariate analysis of X-ray absorption spectroscopy (XAS) data acquired on a set of samples with different Si/Al and Cu/Al composition, pointed to the occurrence of a cooperative process involving proximal Brønsted acid sites during the Cu^{II}/Cu^{I} conversion in inert conditions [16]. Reduction with CO has been shown to selectively reduce dimeric or higher nuclearity Cu-oxo/Cu-hydroxo clusters, without affecting monomeric $Z[Cu^{II}(OH)]$ and Z_2Cu^{II} sites [17], [13].

The Cu^{II}/Cu^{I} reversible transformation plays a fundamental role in the NH_3-SCR cycle, which can be ideally carried out in two half-cycles [18]. NO is reduced to N_2 and H_2O in the presence of NH_3 by a Cu^{II} ion, which is transformed into Cu^{I} and needs to be re-oxidized to complete the cycle. Cu^{II} reduction is thus favored by the presence of NH_3 and, with higher efficiency, of a NO/NH_3 mixture [18-21]. The re-oxidation step is believed to be the kinetically relevant one, since it is characterized by a relatively high activation energy for O_2 dissociation [22-25]. Paolucci et al. recently proposed a reaction pathway 'falling outside the conventional boundaries of a heterogeneous or homogeneous catalyst', since it involves mobile $[Cu^{I}(NH_3)_2]^+$ complexes (formed during reduction with NO/NH_3) which are able to activate O_2 by forming $[Cu^{I}(NH_3)_2\text{-}O_2\text{-}Cu^{I}(NH_3)_2]^{2+}$ pairs [22].

The redox behavior of exchanged Cu ions in CHA has been also recently studied in relation to its catalytic activity in the direct methane to methanol conversion [26-29]. In this context, the formation of mono-copper(II) superoxide species, $Z[Cu^{II}(O_2^{\bullet})]$ during activation in O_2 was also proposed on the basis of XAS and resonance Raman evidences [28]. The authors also studied the formation of Cu-oxo species in different conditions, namely during direct thermal treatment in O_2 or 'decoupling' self-reduction and oxidation processes by contacting the catalyst with O_2 after high temperature activation in inert [28].

Diffuse Reflectance UV-Vis spectroscopy is widely used to study the coordination state and redox cycles of transition metal ion in zeolites [30-37]. As for Cu-zeolites, *ex-situ* results (that is spectra measured at room temperature after activation in controlled atmosphere) on O_2-activated Cu-CHA are characterized by a peculiar absorption in the Visible region (usually assigned to ligand field *d-d* transitions) known as the 'quadruplet'

[10, 12, 38]. This is indeed characterized by a typical shape, with four well-defined components, and by an unusual high intensity. Since *d-d* transitions are Laporte forbidden and usually weak, the high intensity could be related to a highly distorted symmetry and/or by the involvement of ligand centered molecular orbitals. This has been proposed to explain the intense Visible absorption bands of the so-called 'blue-copper' plastocyanin protein, where the Cu^{II} centre is characterized by an elongated C_{3v} geometry with some rombic distortion [39]. On the other hand, Godiksen et al. assigned the quadruplet to EPR active Z_2Cu^{II} sites in 6MR, proposing an approximate trigonal coordination sphere [12]. Interestingly, the quadruplet feature is also observed in few other frameworks, such as Cu-SSZ-16 and Cu-SSZ-39, small pore zeolites which have in common with Cu-CHA the double 6MR framework motif [26]. Very recently, Li et al. used time-dependent DFT calculations to explain the complexity of the Visible 'quadruplet' as the result of *d-d* transitions of monomeric $Z[Cu^{II}(OH)]$ and a variety of Cu-oxo/Cu-hydroxo dimers [13].

Apart from the signals in the Visible region, the most intense spectroscopic features in Cu-zeolites are usually observed above 30000 cm^{-1}, related to ligand to metal charge transfer LMCT transitions ($O^{2-}Cu^{2+} \rightarrow O^{-}Cu^{+}$). Most of recent literature has been focused on the absorption bands between 30000 and 20000 cm^{-1}, which have been assigned to the formation of Cu-oxo species, supposedly active in the selective oxidation of methane to methanol [26, 27, 40-43]. Oord et al. used diffused reflectance (DR) UV-Vis-NIR spectroscopy *ex situ* and in *operando* conditions to address correlations between the Cu sites in Cu-CHA active in this reaction and in NH_3-SCR [29].

Notwithstanding the very interesting results mentioned above, only few works have been reported about a systematic UV-Vis study of the redox properties of Cu^{II}/Cu^{I} sites in Cu-CHA, particularly working *in situ* [29]. Exploiting such conditions has many advantages, since direct information on the structure of metal sites at temperature and chemical conditions relevant for the catalytic application are obtained [44-46]. This approach has been used in this work, where the evolution of Cu oxidation state in Cu-CHA has been followed during activation in O_2 as a function of the temperature and catalyst composition. Moreover, the oxidation process has been 'decoupled' (similarly to what reported by Pappas et al. [28]) to study the interaction with O_2 on a previously self-reduced sample. Finally, resonant Raman spectroscopy, which is the most informative technique for the characterization of Cu-oxo species [41-43, 47-49], has been used *ex situ* to get a more punctual description of the Cu-oxo sites formed in the different conditions.

2. Experimental

The zeolites studied in this paper were provided by Umicore Denmark ApS. The CHA sample with Si/Al =15 was prepared as detailed elsewhere, using aluminum isopropoxide (98%, Sigma-Aldrich), tetraethyl orthosilicate (98% Aldrich) and N,N,N-trimethyl-1-adamantammonium hydroxide (TMAdaOH, 25 wt %, Sachem) as Structure Directing Agent (SDA) in acid solution (hydrofluoric acid) [16]. The resulting gel was placed in a Teflon lined autoclave and hydrothermally treated at 150 °C for 3 days. Calcination was carried out at 500 °C to remove TMAdaOH. For the synthesis of the CHA sample with Si/Al = 5 a sodium silicate solution (26.5 wt % SiO_2, Sigma Aldrich) was mixed with USY (CBV 500) in basic conditions (sodium hydroxide). The resulting gel was placed in a Teflon lined autoclave and hydrothermally treated at 140 °C for 6 days. Calcination was first carried out at 500 °C to remove TMAdaOH and after exchange with ammonium nitrate to obtain the protonic form.
To prepare the corresponding Cu-CHA zeolites, the required amount of copper(II) acetate monohydrate (Sigma-Aldrich, 99.99%) was dissolved in water and the proton form of the zeolite was added to the solution (250 ml per zeolite gram). The solution has been stirred at room temperature for 24h and then the obtained copper zeolite was filtered, washed, dried at 100°C overnight then calcined at 500°C for 3 hours to remove the residual acetate.

Table *1* summarizes the chemical compositions of the two samples.

Sample	Si/Al	Cu/Al	Cu wt%	$Z[Cu^{II}(OH)]$	Z_2Cu^{II}

CHA5_01	5	0.1	1.5	0	1
CHA15_05	15	0.5	2.6	1	0

Table 1– List of samples studied in the current work. The last two columns report the predicted fraction of Z[Cu(OH)] and Z_2-Cu^{II} sites according to Refs. [14, 15].

The *in situ* UV-Vis-NIR spectra were recorded in the 2500-200 nm range (50000-4000 cm^{-1}) at 1 nm resolution (corresponding to 250 and 1.6 cm^{-1} at 50000 and 4000 cm^{-1}, respectively) on a Varian Cary 5000 spectrophotometer, equipped with a R928 PMT UV-Vis detector and a cooled PbS photocell NIR detector. Spectra were collected with a Praying Mantis® element, coupled with a low temperature (LT) reaction chamber. The sample before the measurement was pelletized using a hydraulic press, successively chopped and sieved, selecting for the measurement the fraction between 150 and 300 μm. The reference spectrum was measured at room temperature (RT) using Teflon powder inserted in the same LT cell used for the measurements. Spectra are reported as relative reflectance (R%) defined as:

$$R_{\%} = R_{sample}/R_{reference}$$

Measurements were carried out from RT to 400 °C with a heating ramp of 5°C/min, flowing the desired gases (O_2 or N_2 100 ml/min) with an *ad hoc* built gas flow set-up. The setup consisted of four channels, each of them connected to a specific gas bottle and to a dedicated mass flow controller. The same ramp (5°C/min) was used in the cooling experiments.

The resonant Raman spectra were collected with a Renishaw inVia Raman Microscope spectrometer, operated in backscattering mode and equipped with a He-Cd excitation laser emitting at 442 nm, a 5x objective, a 2400 lines/mm dispersive grating and a Peltier cooled CCD detector. The samples (in powder form, 150-300 μm sieved fraction) were measured within fused silica capillaries (1 mm diameter, 0.01 mm wall thickness), exploited as plug-flow reactors. Thanks to the thin glass wall of the capillaries, their spurious contributions to the Raman spectrum of the samples is negligible. Approximately 1 mg of sample was loaded in each capillary and activated through the same protocols reported above for UV-Vis measurement. The total gas flow was in this case reduced to 10 ml/min according to the lower amount of sample. At the end of each activation procedure, the capillary was sealed from the external environment when still hot (> 200 °C), in order to avoid rehydration processes and thus preserving the Cu-oxo species at RT.

3. Results and discussion

3.1. The starting point: general features of Cu-zeolites UV-Vis-NIR spectra

Before discussing the data obtained during thermal activation (or subsequent cooling and reaction) of the Cu-CHA materials, it could be useful to describe the spectrum of the starting materials as measured before activation. This is reported in Figure 1 for Cu-CHA15_05, a catalyst with 'standard' composition, resulting in an optimal catalytic activity and fully characterized in other works [9-11, 18, 20]. The spectrum in Figure 1 and in the following are here plotted as relative reflectance R%, to avoid the possible artefacts connected to the use of the Kubelka-Munk function [50, 51]. This is particularly important with materials with high absorbance, that is above the theoretical limitations of the Kubelka-Munk theory. Indeed, conversion with this function was reported to give an acceptable correlation with the concentration of absorbing species for R% < 60%, giving on the other hand a serious underestimation for R% > 60% [52, 53]. As exemplified in Figure 1, spectra of Cu-CHA zeolites are characterized by R% spreading in a large range, with values above 60% below *ca* 29000 cm^{-1}. This means that that the relative ratio of CT and *d-d* intensity would be greatly affected by the Kubelka-Munk conversion. Even if we are not attempting a quantitative analysis, it is clear that this could result in artefacts in spectral shape, particularly in the region around 29000 cm^{-1}, where the spectroscopic features of Cu-oxo species are usually observed. Moreover, while measuring the catalysts *in situ*, small changes

in the packing of the pelletized powder as a function of the temperature and/or as an effect of dehydration could affect the sample reflectance and corresponding result [50]. A further warning refers to the fact that the amount of sample measured in the whole spectral range is not constant, reflecting the different penetration depth of the light, being much larger in the NIR region with respect to the ultraviolet. For this reason, when we measure in reflectance, bands in the low energy range (typically *d-d* transitions) become intrinsically stronger, with respect to what they would be if measured in transmission [54].

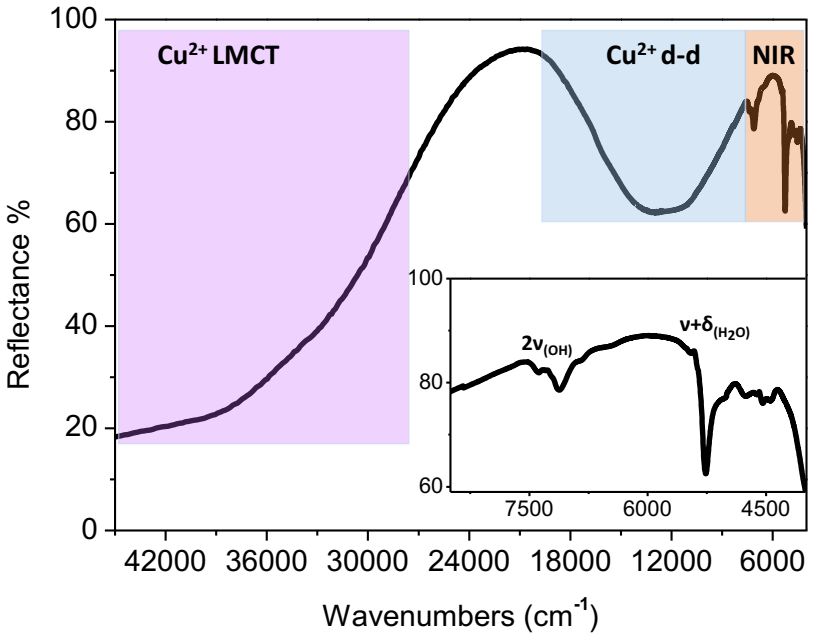

Figure 1. UV-Vis-NIR DR spectrum of hydrated Cu-CHA. The typical LMCT and *d-d* transition regions are highlighted. NIR region is magnified in the inset, with the assignment of the main bands.

Coming back to the description of the spectrum reported in Figure 1, this is characterized by the aforementioned $O^{2-}Cu^{2+} \rightarrow O^{-}Cu^{+}$ LMCT transition, and by a relatively broad an asymmetrical peak related to Cu^{II} ligand field *d-d* ones, centered at 12400 cm^{-1}. The former is characterized by a very high intensity (low relative reflectance) in a spectral range characterized by a low detector sensitivity. This does not allow for a precise and reliable assessment of the bands maximum position. For this reason, in this work LMCT bands will be described in terms of the position of their inflection point, which in the curve shown in Figure 1 is found around R% = 60%.

Similar spectra have been reported for different as-prepared Cu-zeolites, and discussed in terms of hydrated Cu^{II} ions [10]. Notice that the relative intensity of the CT and *d-d* bands reported in this work are very different with respect to *ex situ* spectra on similar samples [10]. This can be related to the different experimental set-up (reflectance sphere *vs* Praying Mantis), further supporting the warning that particular care should be taken while considering the intensity of spectra measured in diffuse reflectance on highly absorbing powders.

Finally, the presence of physisorbed water is confirmed by analysis of the NIR region, below 10000 cm^{-1}, magnified in the inset of Figure 1. This shows a weak group of bands, with maxima at 7400 and 7120 cm^{-1}, related to the overtone of OH stretching modes (ν_{OH}), and a sharp intense peak at 5260 cm^{-1}, assigned to the $\delta+\nu_{asym}$ combination mode of physisorbed water [55]. The analysis of this region will be helpful to check the hydration state of the catalysts during activation and cooling experiments.

3.2. Effect of Si/Al ratio: the state of Cu^{II} ions in the hydrated catalyst

The state of Cu^{II} ions before thermal activation was investigated in samples with different chemical composition, namely Cu-CHA15_05 and Cu-CHA5_01. According to Di Iorio et al., we can assume a random statistical Al distribution in Cu-CHA5_01 (due to the presence of Na^+ ions in the synthesis batch) and isolated Al framework sites in Cu-CHA15-05, thanks to the directing effect of $TMAda^+$ template [15]. This implies that the two activated samples should be characterized by 100% of Z_2Cu^{II} and $Z[Cu^{II}(OH)]$ sites, respectively, as summarized in Table 1.

The zeolites were measured at 50 °C in O_2 flow and are reported in Figure 2. The two spectra show significant differences in the intensity, shape and position of the above described absorptions in the whole UV-Vis-NIR range. In a first approximation, the higher absorbance (lower relative reflectance) of sample Cu-CHA15_05 in the UV-Vis range can be ascribed to its increased Cu loading (2.6 vs 1.5 wt%, see Table 1). However, quantitative considerations should be done with great care, in relation to the scattering contribution to the resulting signal (which is affected by particle size) and because of the uncertainty in the extinction coefficients of the different absorptions. On the other hand, the shape and position of the bands can give important indications on the local environment of the Cu^{II} ions.

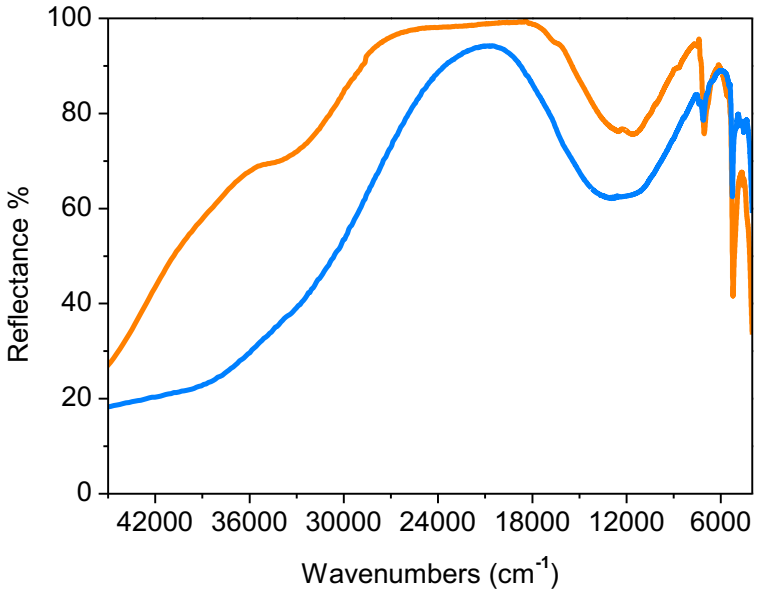

Figure 2. Comparison between UV-Vis-NIR DR spectrum of hydrated Cu-CHA15_05 (light blue curve) and hydrated Cu-CHA5_01 (orange curve). Spectra collected at 50°C in O_2 (100 ml/min)

First, the position of LMCT absorption can be related to the optical electronegativity of the involved ligands and metal centers [56]. Namely, by keeping constant the Cu^{II} metal center, H_2O ligands (lying at the very beginning of the nepheulaxetic series) should result in LMCT bands at higher energy with respect to OH^- and framework oxygen atoms (O_{fr}) [10]. As for the *d-d* bands, these are mainly affected by the coordination environment of the metal center, namely symmetry, number and strength of the ligands.

The reference for the interpretation of these data is the spectrum of Cu^{II} ions in aqueous solution. This is characterized by a high energy LMCT transition (adsorption onset around 40000 cm^{-1}) and by a broad and asymmetric band centered around 12400 cm^{-1}. The latter is explained on the basis of $[Cu^{II}(H_2O)_6]^{2+}$ ions in a distorted octahedral (O_h) coordination, due to Jahn-Teller effect [10]. The same asymmetric band is present on both hydrated Cu-CHA15_05 and Cu-CHA5_01, centered at 12400 and 12200 cm^{-1}, respectively. The main difference between the two materials is the band-width, which is smaller for sample Cu-CHA5_01, indicating a more homogeneous distribution of O_h coordinated Cu ions in the hydrated state.

Moreover, the two catalysts show significantly different LMCT features. Cu-CHA15_05 is characterized by an intense and very broad absorption from 25000 cm^{-1} (inflection point at 28800 cm^{-1}), while Cu-CHA5_01

shows the barycentre of the main LMCT absorption at higher energy and a much less intense component around 30000 cm^{-1}. This suggests a different abundance of the oxygen-based ligands surrounding the O_h coordinated Cu^{II} ions. Based on the position of the LMCT bands, we can infer that in the sample with lower Si/Al ratio $[Cu^{II}(H_2O)_6]^{2+}$ ions are the dominant sites (Scheme 1, left hand structure), stabilized by couples of nearby framework Al atoms. On the other hand, the higher intensity of the lower energy component of the LMCT transition in Cu-CHA15_05 could result from the presence of ligands with higher basicity. This could be tentatively assigned to framework interacting $[Cu^{II}(OH)(H_2O)_5]^{+}$ ions, as proposed by Giordanino et al. [10]. In CuCHA15_05 the presence of an OH^- ligand in the coordination sphere of the partially hydrated Cu^{II} (Scheme 2, left hand structure) is necessary for charge compensation. As mentioned, in this sample Al framework ions are supposed to be isolated, thus not allowing for the stabilization of divalent ions.

The high amount of physisorbed water in Cu-CHA5_01 is also testified by the intensity of the corresponding $\delta+\nu_{asym}$ combination mode in the NIR region (magnified in Figure 3, right hand bottom panel). However, we have to be aware that this fingerprint is not specifically related to water interacting with Cu ions, but is also connected to the high amount of residual Brønsted sites of the sample (see below, Figure 4).

3.3. O_2-activation of Cu-CHA catalysts: effect of Si/Al ratio

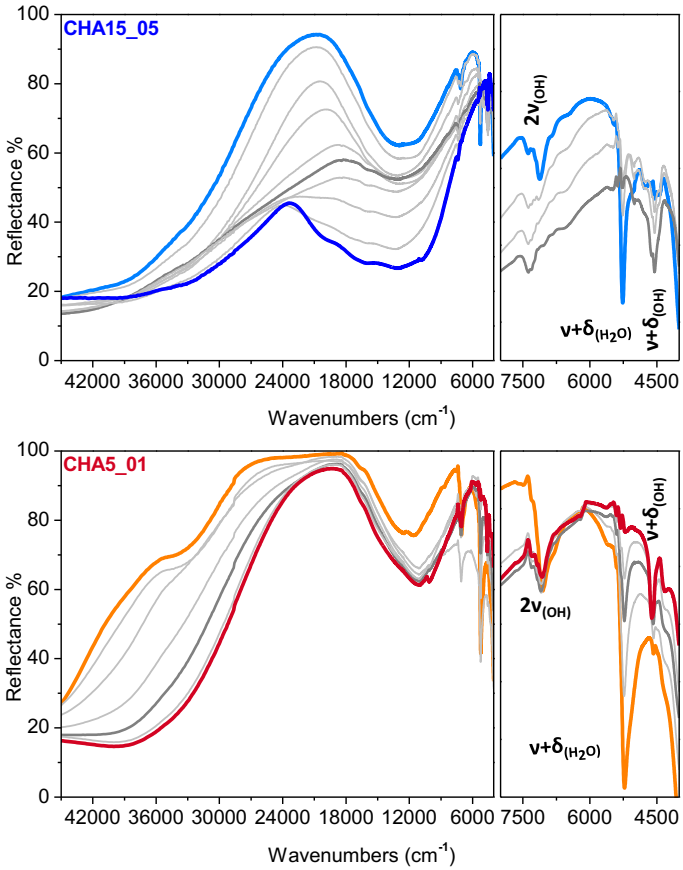

Figure 3. *In situ* UV-Vis-NIR DR spectra of the two Cu-CHA along activation in pure O_2 from 50°C to 400°C. Color code for top panel: light blue thick line: hydrated sample at 50°C; blue thick line: activated sample at 400°C; grey thin lines: intermediates; grey thick line: spectrum at 250°C. Color code for bottom panel: orange thick line: hydrated sample at 50°C; red thick line: activated sample at 400°C; grey thin lines: intermediates; grey thick line: spectrum at 250°C. The right hand panels reported the magnification of the corresponding NIR region.

The evolution of Cu-CHA spectra upon activation in O_2 in the 50-400 °C range is reported in Figure 3 for Cu-CHA15_05 and Cu-CHA5_01 (top and bottom panels, respectively). Based on the findings by Di Iorio et al. and the Cu site compositional phase diagram proposed by Paolucci et al., after O_2-activation these should be

characterized by $Z[Cu^{II}(OH)]$ and Z_2Cu^{II} sites, respectively [14, 15]. This hypothesis is consistent with previously reported experimental data (XAS and FTIR) [9, 10, 16].

Upon activation, both samples show an important change in the LMCT range, which can be described as a red-shift, which can be interpreted in terms of changes of ligands in the coordination sphere of the Cu^{II} ions. As a first approximation, we can describe the changes assuming the evolution from an ionic (H_2O-based) to a more covalent bonding environment, resulting in framework coordinated Cu^{II} ions [10]. The two catalysts show a different behavior with respect to the dehydration process. In the case of Cu-CHA15_05 complete removal of physisorbed water molecules is observed around 250 °C, as testified by the disappearance of the $\delta+\nu_{asym}$ combination mode at 5260 cm^{-1} in the NIR region (thick grey curve, see magnification in Figure 3, left hand top panel). This is accompanied by the modification of the ν_{OH} (7330 cm^{-1}) and corresponding $\nu+\delta$ combination mode at 4560 cm^{-1}, related to silanols and Brønsted groups previously interacting by hydrogen bond with water molecules. This is in agreement with previous reports about catalysts with similar composition [9]. On the other hand, at the same temperature Cu-CHA5_01 still shows a significant amount of physisorbed water, which is totally desorbed only at 400 °C (see NIR magnification in right hand bottom panel of Figure 3). This observation, in agreement with what discussed in the previous paragraph, can be easily explained on the basis of the high Al content of the sample, resulting in high hydrophilic character.

In Cu-CHA5_01 the *d-d* band (initially centered at 12200 cm^{-1}) increases in intensity and shifts to lower frequency (maximum around 11200 cm^{-1}) after complete dehydration at 400 °C. Interestingly, in these conditions, the shape of the peak is quite similar to that observed in the hydrated state, assigned to framework stabilized $[Cu^{II}(H_2O)_6]^{2+}$ ions. This is at variance with what usually observed on O_2-activated Cu-CHA materials, which are characterized by the typical quadruplet, with components at 19700, 16500, 13600 and 11000 cm^{-1} (as measured in *ex situ* conditions at RT) [10, 26, 27, 29].

Based on the predictions by Paolucci et al., we can assume that the predominant sites formed upon O_2-activation in this sample are Z_2Cu^{II} sites, stabilized in the 6MR [14, 16]. The coordination geometry of Cu^{II} ions in these structures can be described as square-planar [13]. Noticeably, the $[Cu^{II}(H_2O)_6]^{2+}$ ions present at the onset of thermal activation are expected to be characterized by a distorted octahedral configuration due to the Jahn-Teller effect. This can be described with four in-plane H_2O molecules strongly bonded to the metal ions and two farther, less interacting ones along the z axis [10]. We can thus assume that the two axial molecules are the first to be desorbed, resulting in square-planar partially hydrated ions described as $[Cu^{II}(H_2O)_4]^{2+}$ by Martini et al. [16], finally evolving into Z_2Cu^{II} sites at 400°C. This transformation (pictorially depicted in Scheme 1) is in agreement with the observed changes in CT position (due to change in the nature of O ligands from water to framework atoms) and small change in d-d shape and position, implying minor changes in Cu^{II} local symmetry and crystal field. These observations are in good agreement with the recent report by Li et al., who calculated the UV-Vis spectrum of 'meta' and 'para' Z_2Cu^{II} sites in 6MR [13].

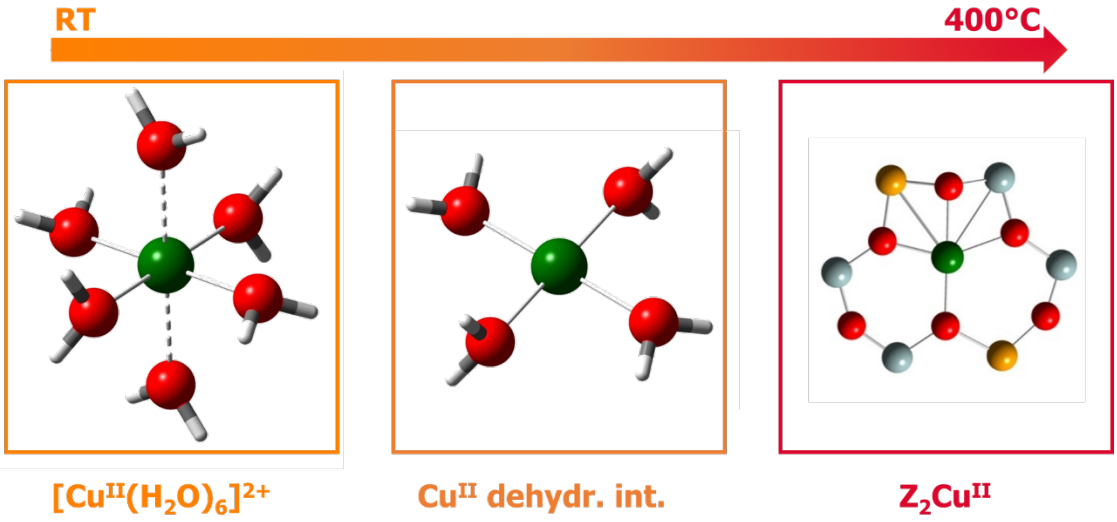

Scheme 1. Pictorial representation of the evolution of the Cu^{II} environment along activation in O_2 (50-400 °C) in Cu-CHA5_01.

On the contrary, in Cu-CHA15_05 an important modification in the local symmetry of Cu^{II} ions during dehydration is testified by the shape and intensity of the *d-d* bands growing in the 250-400 °C range. This can be described as a quadruplet, with components at 20400, 16500, 13200 and 10400 cm^{-1}, reaching its higher intensity and better spectral definition at 400 °C. The anomalously high intensity of these bands, responsible for the intense blue colour of O_2-activated Cu-CHA, can be explained with a highly distorted symmetry of the corresponding metal centre. It is thus reasonable to assign these features to $Z[Cu^{II}(OH)]$ ions, where the metal ion has a trigonal coordination (distorted *C3v*) with two equivalent framework oxygen atoms and a shorter Cu-OH bond [9]. Notice that this configuration is similar to that of Cu ions in plastocyanin, which are characterized by a very intense and complex absorption centred at 16000 cm^{-1}. The high intensity was explained on the basis of the good overlap between ground state antibonding dx^2-dy^2 orbitals and the bonding Sπ excited state of a cysteine ligand [39]. We want to stress the fact that the relative intensity and position the quadruplet components show variability in samples with different chemical composition of 'preparation history' (not reported here for the sake of brevity). This suggests the presence of a distribution of Cu^{II} sites with similar but not identical local environment. Li et al. have explained this variability by the presence of $Z[Cu^{II}(OH)]$ ions (responsible for some of the bands typical of the quadruplet) and by a plethora of dimeric and higher nuclearity Cu-oxo and Cu-hydroxo clusters [13]. In other words, the well-known quadruplet cannot be assigned to a single structural motif but to the presence of a complex mixture of Cu^{II} sites, stabilized by a single framework negative charge, with relative concentration strongly depending upon the activation conditions in O_2.

The presence of a variety of different framework coordinated Cu^{II} sites with distorted *C3v* symmetry in Cu-CHA15_05 catalysts is also suggested by the complex changes in the CT region, in the temperature range corresponding to the quadruplet evolution (250 – 400 °C). Namely, a broad absorption grows above 24000 cm^{-1}, with concomitant decrease of the LMCT intensity above 38700 cm^{-1}, and formation of an apparent isosbestic point. This indicates a change in the ligands coordinated to the Cu^{II} center, while its local symmetry is preserved. The spectral region between 35000 and 20000 cm^{-1} is characteristic of a variety of mononuclear and binuclear Cu_xO_y complexes [48, 49]. Many studies have been focused on these features to assess the precise structure of Cu-oxo sites active in selective oxidation reactions, such as the direct methane to methanol conversion [26, 27, 29, 40-43, 57]. For instance, Ipek et al. assigned a broad absorption in the 35000 - 22200 cm^{-1} range to the contribution of trans-μ-1,2-peroxo and mono(μ-oxo) dicopper structures stabilized in the CHA framework [27]. Based on the broadness of the features observed in this work, we are not able to precisely assign them to a specific $Z_2[Cu_2O_y]$ core. However, we would like to stress the fact that in most of these structures the involved Cu^{II} centers could maintain the distorted *C3v* symmetry proposed for $Z[Cu^{II}(OH)]$ ions, due to the coordination to two equivalent O_{fr} and the addition of a third O_2-based ligand.

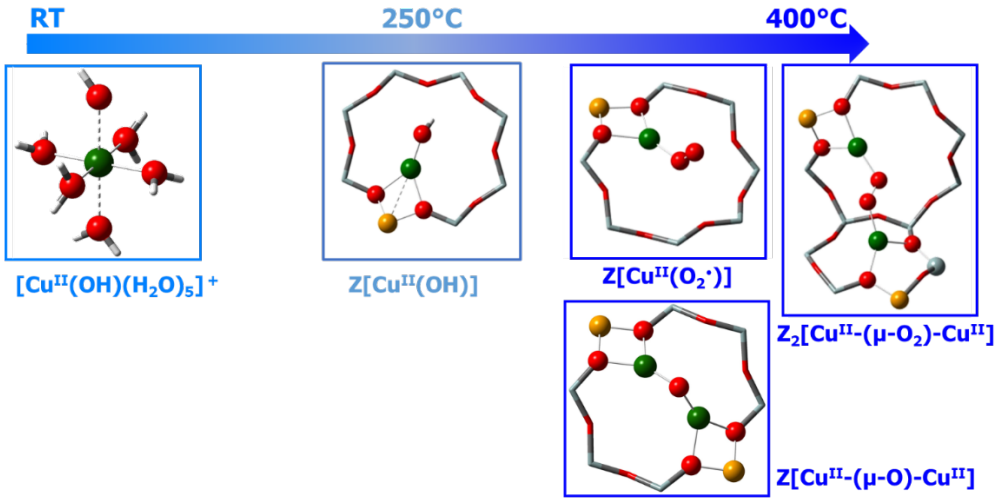

Scheme 2. Pictorial representation of the evolution of the Cu^{II} environment along activation in O_2 (50-400 °C) in Cu-CHA15_05.

We thus propose, for Cu-CHA15_05 catalyst, the dehydration process depicted in Scheme 2. Namely, we can assume the presence of (a consistent fraction of) $[Cu^{II}(OH)(H_2O)_5]^+$ sites, stabilized by one negative charge on the framework. Upon dehydration in O_2, in agreement with previous reports [9], $Z[Cu^{II}(OH)]$ sites starts to develop around 250 °C, giving the characteristic quadruplet in the *d-d* region. In the 250 -400 °C, the $Z[Cu^{II}(OH)]$ sites react with O_2 to give a variety of $Z_2[Cu_2O_y]$ cores, contributing to the intensity and broadness of the quadruplet and responsible for the broad absorption in the 36000 – 24000 cm^{-1}. Scheme 2 reports some examples of the possible Cu-oxo structure formed in these conditions, including the $Z[Cu^{II}(O_2^{\bullet})]$ superoxo site proposed by Pappas et al. on the basis of Raman evidences [28]. As mentioned above, on the basis of the UV-Vis results, we are not able to give a precise assessment of the Cu-oxo species formed in these conditions. However, our results clearly indicate a dynamic interplay between the $Z[Cu^{II}(OH)]$ sites and mononuclear or dinuclear Cu-oxo moieties.

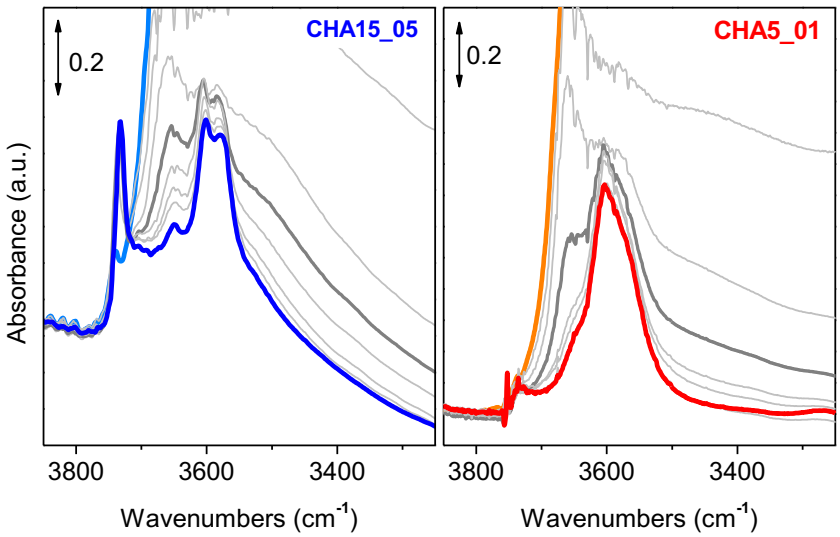

Figure 4. *In situ* FTIR spectra of Cu-CHA during activation in pure O_2 from 50°C to 400°C. Color code for left panel: light blue thick line: hydrated sample at 50°C; blue thick line: activated sample at 400°C; grey thin lines: intermediates; grey thick line: spectrum at 250°C. Color code for right panel: orange thick line: hydrated sample at 50°C; red thick line: activated sample at 400°C; grey thin lines: intermediates; grey thick line: spectrum at 250°C.

Further support to the interpretation of the above-described UV-Vis spectra can be obtained from analysis of FTIR spectra collected in similar conditions (Figure 4). The spectra of Cu-CHA15_05 during O_2-activation are similar to what already reported and discussed in the literature [9, 28]. Namely, in the 3800 to 3500 cm^{-1} range the typical νOH modes of silanols (3737 cm^{-1}) and residual Brønsted acid sites (3611 and 3584 cm^{-1}) are observed in the 250-400 °C range (dark grey to blue curves). The band around 3650 cm^{-1}, identified as the fingerprint of $Z[Cu^{II}(OH)]$ sites, gradually decreases with temperature but is still partially visible at 400 °C [10]. This observation is in agreement with the dynamic evolution of $Z[Cu^{II}(OH)]$ sites into Cu-oxo species in the studied temperature range. On the other hand, the infrared spectra of Cu-CHA5_01 catalyst are characterized by a significantly higher intensity of the ν(OH) mode of Brønsted acid groups, in agreement with its low Si/Al ratio. Above 250 °C, no evidence for the presence of the typical fingerprint of $Z[Cu^{II}(OH)]$ sites is observed, in agreement with the expected predominance of Z_2Cu^{II} sites. The analysis of the fingerprint of physisorbed water at 1625 cm^{-1} (not reported here for brevity) confirms the higher hydrophilicity of Cu-CHA5_01 with respect to Cu-CHA15_05. Namely, above 250°C this feature is still present with significant intensity on the former, while it disappears on the latter.

It is interesting at this point to discuss the effect of temperature on the $Z[Cu^{II}(OH)]$ and framework interacting Cu-oxo species formed by O_2-activation at 400 °C. This was followed by cooling Cu-CHA15_05 in O_2 flow down to 200 °C (Figure 5). This temperature was selected since representative for the reactivity conditions of the catalysts in both NH_3-SCR and methane to methanol reactions [18, 22, 26-29, 42, 43, 57]. The main changes

are observed in the CT region, with a gradual decrease of the broad absorption between 36000 and 24000 cm^{-1}, and concomitant increase at higher energy. This transformation is again indicating a change in the nature of the oxygen ligands surrounding the Cu^{II} ions. This is not accompanied by a substantial decrease of the overall *d-d* intensity between 400 and 250 °C, pointing out as that the local geometry of the metal center is maintained. We can thus infer that in this temperature range the previously described transformation of $Z[Cu^{II}(OH)]$ to $Z_2[Cu_2O_y]$ (Scheme 2) is partially reversible.

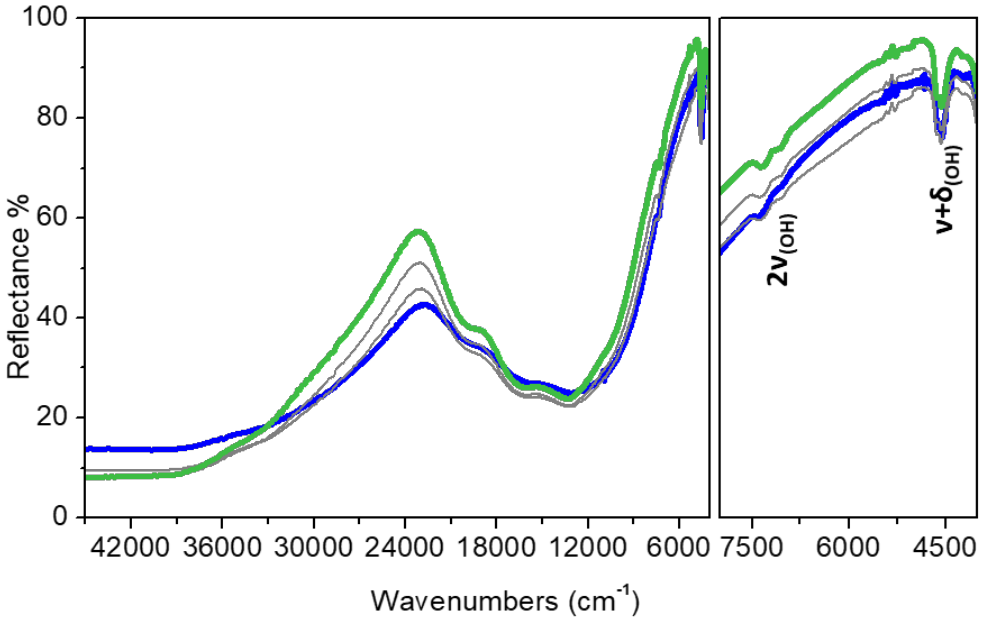

Figure 5. *In situ* UV-Vis-NIR DR spectra of Cu-CHA15_05 during cooling in O_2 from 400°C to 200°C after activation in O_2. Colour code: blue thick line: oxidized sample at 400°C; green thick line: oxidized sample at 200°C; grey thin lines: intermediates. The right hand panel reports the magnification of the corresponding NIR region.

3.4. Cu^{II} reduction in inert atmosphere

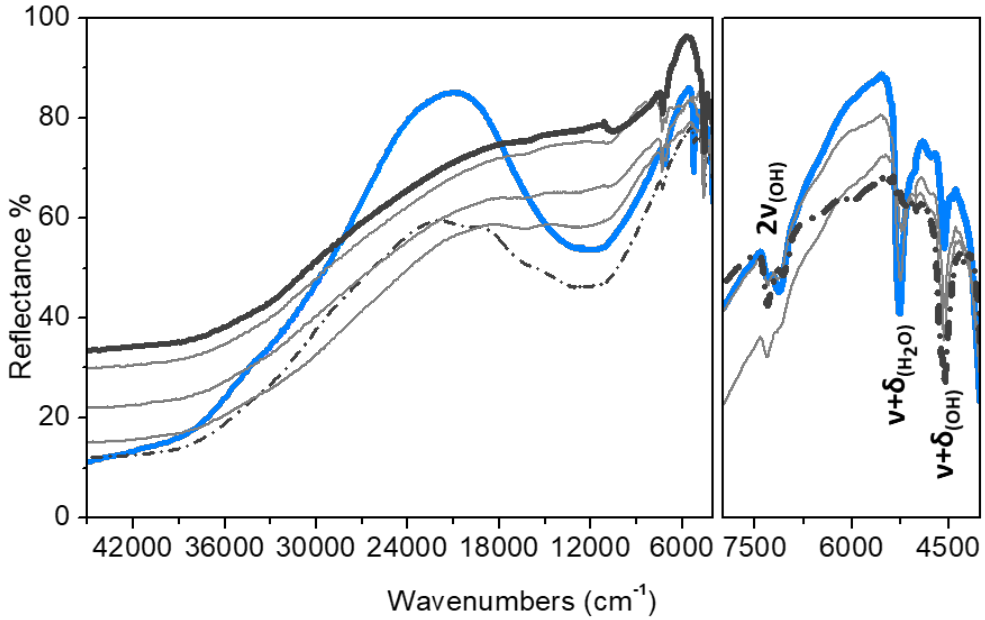

Figure 6. *In situ* UV-Vis-NIR DR spectra of Cu-CHA15_05 during activation in N_2 from 50 °C to 400 °C, heating rate 5°C/min. Color code: light blue thick line: hydrated sample at 50 °C; dark grey thick line: activated sample at 400 °C; grey thin lines: intermediate; dashed dark grey line: spectrum with maximum intensity of the quadruplet (200 °C). The right hand panels reported the magnification of the corresponding NIR region.

The activation of Cu-CHA15_05 was also followed in inert conditions (N_2 flow), in order to investigate the 'self-reduction' dynamics [9, 58]. Observing the spectra obtained during this experiment (Figure 6), two different behaviours can be distinguished as a function of temperature. In the 50-200 °C range, we observe an initial evolution of the spectra comparable to what previously observed during O_2 activation. Starting from the hydrated state previously described, we observe a red-shift of the LMCT transition, associated with the change of ligands coordinated with Cu^{II} ions and the development of the intense quadruplet bands in the *d-d* region. This feature reaches its maximum intensity at 200 °C (dashed dark grey curve in Figure 6), temperature which is associated with the complete dehydration of the catalyst surface, as visible from the NIR region, magnified in the right hand panel of Figure 6. Here we can clearly observe that the signal at 5260 cm^{-1} related to the presence of physisorbed water molecules progressively decrease, until the completely disappearance of these features by reaching 200 °C. This is accompanied by the growth of the ν(OH) and ν+δ combination modes of 'free' silanols and Brønsted sites (7330 and 4560 cm^{-1}). It is worth noticing that, under the applied conditions, the dehydration process occurs more efficiently with respect to the oxidizing atmosphere, where physisorbed water is completely depleted at 250 °C. This suggests that water plays an important role in the mechanisms leading to framework interacting Cu^{II} and Cu^{I} ions.

Above 200 °C (grey curves in Figure 6), the intensity of the quadruplet progressively decreases, indicating the reduction of Cu^{II} to Cu^{I}. Indeed, *d-d* transitions are not possible in Cu^{I} ions, owing to their d^{10} electronic configuration. This gradual transformation is complete at 400 °C, when the spectrum is characterized by an almost flat line in the *d-d* region (the weak peak visible around 10000 cm^{-1} can be related to bad background compensation at 400°C). This observation (never reported with this technique to our knowledge in case of chabazite) is in agreement with previous XAS studies about Cu-CHA activation in inert conditions [9, 16]. The mechanism for this transformation, the so-called 'self-reduction' has been explained as a consequence of oxygen based extra-ligand loss from $Z[Cu^{II}OH]$ sites, written as follows [9, 14, 59, 60]:

$$Z[Cu^{II}(OH)(H_2O)_n]^+ \rightarrow Z[Cu^{II}OH]^+ + n(H_2O)^{\uparrow} \rightarrow Cu^{I} + (OH)^{\uparrow}$$

This mechanism is here mentioned for the relatively low temperature at which reduction occurs and since it can explain the virtually complete Cu^{II} to Cu^{I} transformation, at variance with other mechanisms proposed in literature ([58] and references therein). In parallel with the *d-d* bands disappearance, a gradual blue-shift of the LMCT transitions can be observed. This is in agreement with what expected on the basis of the variation of the optical electronegativity of Cu^{I} compared to Cu^{II}, keeping constants the oxygen-based ligands [56]. However, it is important to remember that Cu^{I} ions in zeolites are luminescent in the visible region, being characterized by a variety of components between 450 to 550 nm, reflecting the local environment of the copper species. [61-64] This implies that the measured reflectance spectra in that corresponding region, could be affected by the presence of luminescence effects.

As a final remark, it is worth mentioning the interesting work by Suskevich and van Bokhoven, who recently revisited the 'self-reduction' mechanism, invoking the role of traces of carbonaceous impurities in the Cu^{II} to Cu^{I} transformation in inert conditions [58]. Indeed, the results reported in Figure 6 were obtained starting from a catalyst calcined after the synthesis, which could have adsorbed organic compounds from air before the experiment. Repeated oxidation/inert activation cycles (not reported) resulted in a less efficient reduction, supporting the observations from the above-mentioned authors.

3.5 Comparing direct O_2 activation with O_2-reactivity on Cu^I

Following the result obtained after thermal activation in inert conditions, we have investigated the reactivity of the obtained Cu^{I} ions towards O_2. The aim of the experiment is to compare the Cu^{II} and Cu-oxo species formed by direct dehydration in O_2 (that is in the presence of water, adsorbed on the catalyst surface up to 250 °C), with that of previously reduced Cu^{I} ions in absence of water traces.

Thus, the reduced catalyst has been exposed to pure O_2 at 400°C. The final state after one-hour interaction is directly compared in Figure 7 with that of the O_2-activated catalyst (light pink and blue thick lines, respectively). No significant differences are visible between the spectra of the two final states: both the quadruplet and the LMCT features present in the oxidized state are completely restored upon exposure of the Cu^{I}-moieties to O_2. From these findings, we can infer that the species formed during the re-oxidation of Cu^{I} at high temperature are comparable from electronic point of view, to those present during O_2 activation.

In the previous Section, we have proposed the formation of different Cu-oxo species with a similar local structure, evolving from $Z[Cu^{II}OH]^{+}$ sites at temperature sufficiently high. These results indicate that the same species are here formed upon direct interaction of O_2 molecules with reduced Cu ions.

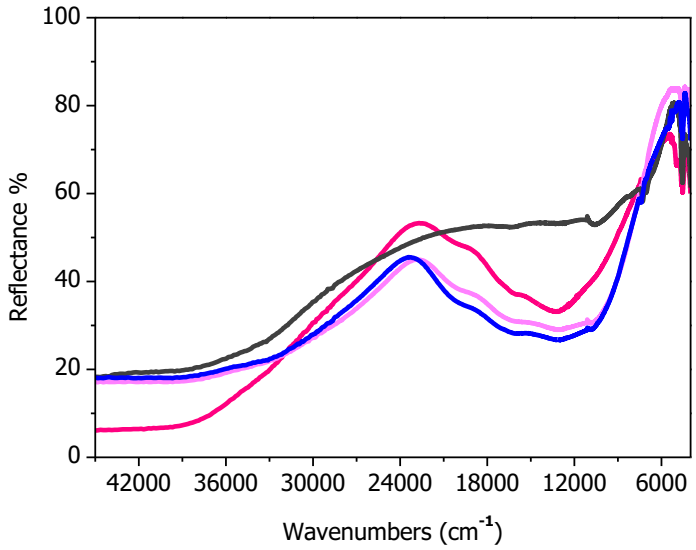

Figure 7. Comparison among UV-Vis-NIR DR spectra of different Cu-CHA15_05 states. Color code: dark grey line: reduced sample at 400°C after N_2 activation; blue line: oxidized sample at 400°C after O_2 activation; pink line: re-oxidized sample obtained after exposure of the reduced catalyst to pure O_2 at 400°C; dark pink line: re-oxidized sample cooled to 200°C.

Furthermore, we have investigated the effect of cooling on the re-oxidized catalyst, reported as dark rose curve in Figure 7. As visible from the curve reported, the catalyst behaves as previously observed during cooling of the oxidized catalyst (Figure 5). In fact, we again observe a gradual decrease in the broad absorption between 36000 and 24000 cm^{-1}, and concomitant increase at higher energy, associated with a change in configuration of the formed Cu-oxo complexes. This indicates that the species formed during Cu^{I} re-oxidation at high temperature show a similar stability to those formed during direct O_2 activation.

3.6 Addressing the nature of Cu-oxo species by resonant Raman spectroscopy

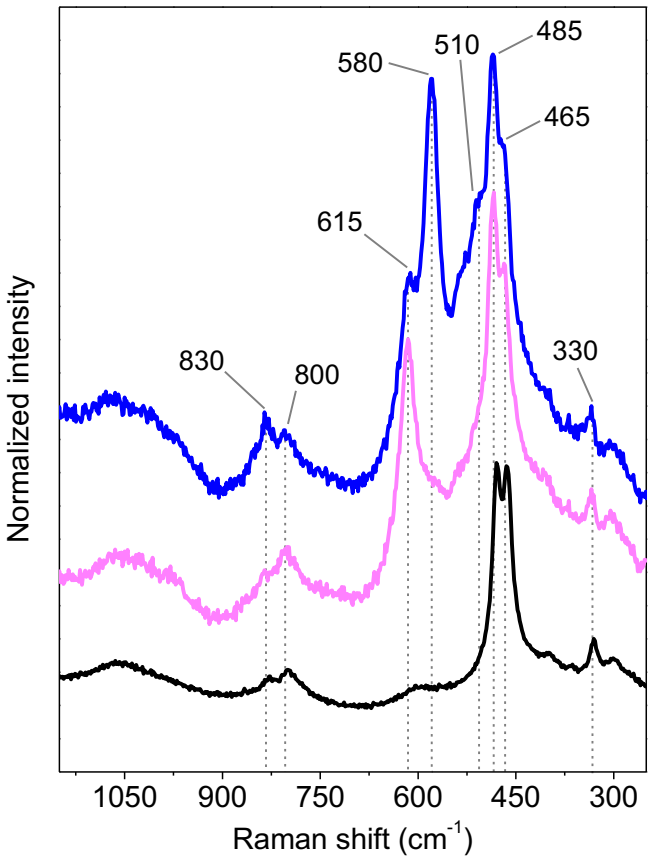

Figure 8. Comparison of Raman spectra (λ = 442 nm) of Cu-CHA15_05 sample activated in different conditions. Color code: blue curve: direct activation from RT to 400 °C in pure O_2. Pink curve: activation in inert at 400 °C, followed by O_2 exposure at the same temperature. Black curve: spectrum of the hydrated sample, reported for the sake of comparison. All the spectra have been collected at RT and their intensity was normalized to the one of the 330 cm^{-1} vibrational mode of chabazite framework.

In order to explore the speciation of the Cu-oxo sites, resonant Raman has been applied according to its superior sensitivity toward these moieties [27, 28]. In detail, we focused the attention on Cu-CHA15_05 sample in relation to its complex dynamics as discussed in the previous Sections (Figure 8). In the Raman spectrum of the hydrated material, no signals ascribable to Cu-moieties are observed and all the main features relate to the framework vibrational modes of chabazite [65]. Many of these (including the intense doublet of bands at 485 and 465 cm^{-1}) are expected to partially overlap with the fingerprints of the Cu-oxo species, whereas this is not the case of the weak but sharp and isolated peak at 330 cm^{-1}. For this reason, the latter has been exploited for the intensity normalization of the spectra, allowing a relative quantitative comparison to be performed.

The attention was focused on the effect of O_2-activation *vs* O_2 re-oxidation of the Cu-CHA15_05 reduced sample. In both cases similar Cu-oxo species are observed. However, their speciation differs depending on the oxidation state of Cu at the beginning of the high temperature oxidation. Starting from a 'self-reduced' Cu^{I} state, upon exposure to O_2 at 400 °C, a sharp feature is observed at 615 cm^{-1}. According to Ipek and coworkers and references herein [27], this feature can be ascribed either to $[Cu^{II}\text{-}(\mu\text{-}O)\text{-}Cu^{II}]^{2+}$ or $[Cu^{III}\text{-}\textit{bis}\text{-}(\mu\text{-}O)\text{-}Cu^{III}]^{2+}$ μ-oxo dicopper cores. However, our previous XAS investigation on the same material in analogous activation conditions demonstrated the absence of Cu^{III} [28], thus the 615 cm^{-1} peak can be reasonably ascribed to $[Cu^{II}\text{-}(\mu\text{-}O)\text{-}Cu^{II}]^{2+}$.

On the other hand, by directly activating the sample in O_2 (similarly to what reported in Figure 3), an increased number of features is observed. The 615 cm^{-1} peak presents a similar intensity compared to the previous case. Moreover, we observe a very intense peak at 580 cm^{-1}, accompanied by a weaker one at 830 cm^{-1} and by a shoulder at 510 cm^{-1}. Still referring to Ipek et al. [27], these signals univocally relates to the formation of $[Cu^{II}\text{-}$

trans-(μ-*1,2*-O_2)-$Cu^{II}]^{2+}$ peroxo moiety, which were reported to be dominant in samples activated in fully oxidizing conditions [28]. Concerning monomeric Cu-oxo species, the weak and broad features observed in the 1000-1100 cm^{-1} range could be related to the formation of $[Cu^{II}O_2^{\bullet}]^+$ superoxo species [28, 42, 66, 67]. However, due to their low intensity, these are most probably overlapping with the emission from residual carbonaceous impurities, not completely removed during the activation treatments. The assignment of this band to Cu-superoxo in this work is thus not conclusive.

Remarkably, resonant Raman measurements showed the different oxidative behavior depending on the initial oxidation state of the Cu ions in the dehydrated zeolite. The results highlight as the formation of dinuclear $[Cu^{II}$-*trans*-(μ-1,2-O-O)-$Cu^{II}]^{2+}$ peroxo type of species is favored in the presence of dehydrated Cu^{II} sites, whereas $[Cu^{II}$-(μ-O)-$Cu^{II}]^{2+}$ are formed in similar amounts on both Cu^{I} and Cu^{II} during high temperature oxidation. Notice that these structures were proposed to be responsible for the broad absorption between 35000 and 2200 cm^{-1}, in agreement with our UV-Vis results [27].

4. Conclusions

In situ UV-Vis-NIR spectroscopy was used to study the evolution of Cu^{II} ions inserted in CHA frameworks by ion exchange during dehydration in O_2 or inert atmosphere. This technique allowed us observing differences in the coordinated state of Cu^{II} ions in hydrated Cu-CHA catalysts with different chemical composition. Namely, the Si/Al ratio was found to affect both hydrophilicity of the material and the number of aquo ligands solvating Cu^{II} ions. Upon O_2-activation, the changes observed on the sample with low Si/Al ratio could be interpreted as a gradual loss of water ligands resulting in Cu^{II} ions stabilized in the 6MR by two negative framework charges (Z_2Cu^{II}). On the other hand, in the sample with higher Si/Al ratio (Cu-CHA15_05), the appearance of the well-known quadruplet was explained in terms of the formation of Cu^{II} ions in distorted C_{3v} symmetry. These can be described as Cu^{II} ions coordinated to two equivalent framework oxygen atoms and to an O-based extra ligand. This could be an OH^-, resulting in $Z[Cu^{II}OH]^+$ sites, superoxo groups in $[Cu^{II}O_2^{\bullet}]^+$, peroxo ones in dinuclear $[Cu^{II}$-*trans*-(μ-1,2-O-O)-$Cu^{II}]^{2+}$ complexes and single oxygen atoms in $[Cu^{II}$-(μ-O)-$Cu^{II}]^{2+}$ cores. The presence of these Cu-oxo sites is responsible for a broad adsorption in the 36000-24000 cm^{-1} range, growing above 250 °C. The same spectral features were observed by reaction of O_2 in water free conditions with Cu^{I} ions obtained by activation in inert atmosphere.

UV-Vis-NIR DR spectroscopy allowed us following the dynamics of the Cu-oxo formation and stability with temperature and to follow the Cu^{II} to Cu^{I} reduction during dehydration in inert conditions. However, this technique does not provide a clear indication about the speciation of the Cu-oxo structures formed in temperature. Thus we used resonant Raman spectroscopy to unravel the structure of Cu-oxo structures formed in the different conditions, that is direct dehydration in O_2 vs O_2 exposure at high temperature of "self-reduced" catalyst. Remarkably, this technique showed that $[Cu^{II}$-(μ-O)-$Cu^{II}]^{2+}$ cores are formed irrespective of the starting Cu oxidation state. On the hand, $[Cu^{II}$-*trans*-(μ-1,2-O-O)-$Cu^{II}]^{2+}$ peroxo are favored during the O_2-dehydration process. Finally, the formation of $[Cu^{II}O_2^{\bullet}]^+$ superoxo complexes cannot be ascertained.

References

[1] J.H. Kwak, R.G. Tonkyn, D.H. Kim, J. Szanyi, C.H.F. Peden, J. Catal. 275 (2010) 187-190.
[2] S.J. Schmieg, S.H. Oh, C.H. Kim, D.B. Brown, J.H. Lee, C.H.F. Peden, D.H. Kim, Catal. Today. 184 (2011) 252-261.
[3] F. Gao, E.D. Walter, E.M. Karp, J. Luo, R.G. Tonkyn, J.H. Kwak, J. Szanyi, C.H.F. Peden, J. Catal. 300 (2013) 20-29.
[4] F. Gao, J.H. Kwak, J. Szanyi, C.H.F. Peden, Top. Catal. 56 (2013) 1441-1459.
[5] A.M. Beale, F. Gao, I. Lezcano-Gonzalez, C.H.F. Peden, J. Szanyi, Chem. Soc. Rev. 44 (2015) 7371-7405.
[6] F. Goltl, R.E. Bulo, J. Hafner, P. Sautet, J. Phys. Chem. Lett. 4 (2013) 2244-2249.
[7] J.H. Kwak, T. Varga, C.H.F. Peden, F. Gao, J.C. Hanson, J. Szanyi, J. Catal. 314 (2014) 83-93.
[8] J.H. Kwak, H.Y. Zhu, J.H. Lee, C.H.F. Peden, J. Szanyi, Chem. Commun. 48 (2012) 4758-4760.
[9] E. Borfecchia, K.A. Lomachenko, F. Giordanino, H. Falsig, P. Beato, A.V. Soldatov, S. Bordiga, C. Lamberti, Chem. Sci. 6 (2015) 548-563.
[10] F. Giordanino, P.N.R. Vennestrom, L.F. Lundegaard, F.N. Stappen, S. Mossin, P. Beato, S. Bordiga, C. Lamberti, Dalton T. 42 (2013) 12741-12761.
[11] C.W. Andersen, E. Borfecchia, M. Bremholm, M.R.V. Jorgensen, P.N.R. Vennestrom, C. Lamberti, L.F. Lundegaard, B.B. Iversen, Angew. Chem. Int. Edit. 56 (2017) 10367-10372.
[12] A. Godiksen, F.N. Stappen, P.N.R. Vennestrom, F. Giordanino, S.B. Rasmussen, L.F. Lundegaard, S. Mossin, J. Phys. Chem. C. 118 (2014) 23126-23138.
[13] H. Li, C. Paolucci, I. Khurana, L. Wilcox, F. Goltl, J.D. Albarracin-Caballero, A.J. Shih, F.H. Ribeiro, R. Gounder, W.F. Schneider, Chem. Sci. 10 (2019) 2373-2384.
[14] C. Paolucci, A.A. Parekh, I. Khurana, J.R. Di Iorio, H. Li, J.D. Albarracin Caballero, A.J. Shih, T. Anggara, W.N. Delgass, J.T. Miller, F.H. Ribeiro, R. Gounder, W.F. Schneider, J. Am. Chem. Soc. 138 (2016) 6028-6048.
[15] J.R. Di Iorio, R. Gounder, ACS Chem. Mater. 28 (2016) 2236-2247.
[16] A. Martini, E. Borfecchia, K.A. Lomachenko, I.A. Pankin, C. Negri, G. Berlier, P. Beato, H. Falsig, S. Bordiga, C. Lamberti, Chem. Sci. 8 (2017) 6836-6851.
[17] P. Da Costa, B. Moden, G.D. Meitzner, D.K. Lee, E. Iglesia, Phys. Chem. Chem. Phys. 4 (2002) 4590-4601.
[18] T.V.W. Janssens, H. Falsig, L.F. Lundegaard, P.N.R. Vennestrøm, S.B. Rasmussen, P.G. Moses, F. Giordanino, E. Borfecchia, K.A. Lomachenko, C. Lamberti, S. Bordiga, A. Godiksen, S. Mossin, P. Beato, ACS Catal. 5 (2015) 2832-2845.
[19] I. Lezcano-Gonzalez, U. Deka, B. Arstad, A. Van Yperen-De Deyne, K. Hemelsoet, M. Waroquier, V. Van Speybroeck, B.M. Weckhuysen, A.M. Beale, Phys. Chem. Chem. Phys. 16 (2014) 1639-1650.
[20] K.A. Lomachenko, E. Borfecchia, C. Negri, G. Berlier, C. Lamberti, P. Beato, H. Falsig, S. Bordiga, J. Am. Chem. Soc. 138 (2016) 12025-12028.
[21] A.G. Greenaway, I. Lezcano-Gonzalez, M. Agote-Aran, E.K. Gibson, Y. Odarchenko, A.M. Beale, Top. Catal. 61 (2018) 175-182.
[22] C. Paolucci, I. Khurana, A.A. Parekh, S.C. Li, A.J. Shih, H. Li, J.R. Di Iorio, J.D. Albarracin-Caballero, A. Yezerets, J.T. Miller, W.N. Delgass, F.H. Ribeiro, W.F. Schneider, R. Gounder, Science. 357 (2017) 898-+.
[23] L. Chen, H. Falsig, T.V.W. Janssens, H. Gronbeck, J. Catal. 358 (2018) 179-186.
[24] L. Chen, H. Falsig, T.V.W. Janssens, J. Jansson, M. Skoglundh, H. Gronbeck, Catal. Sci. Technol. 8 (2018) 2131-2136.
[25] A. Marberger, A.W. Petrov, P. Steiger, M. Elsener, O. Krocher, M. Nachtegaal, D. Ferri, Nat. Catal. 1 (2018) 221-227.
[26] M.J. Wulfers, S. Teketel, B. Ipek, R.F. Lobo, Chem. Commun. 51 (2015) 4447-4450.
[27] B. Ipek, M.J. Wulfers, H. Kim, F. Goltl, I. Hermans, J.P. Smith, K.S. Booksh, C.M. Brown, R.F. Lobo, ACS Catal. 7 (2017) 4291-4303.
[28] D.K. Pappas, E. Borfecchia, M. Dyballa, I.A. Pankin, K.A. Lomachenko, A. Martini, M. Signorile, S. Teketel, B. Arstad, G. Berlier, C. Lamberti, S. Bordiga, U. Olsbye, K.P. Lillerud, S. Svelle, P. Beato, J. Am. Chem. Soc. 139 (2017) 14961-14975.
[29] R. Oord, J.E. Schmidt, B.M. Weckhuysen, Catal. Sci. Technol. 8 (2018) 1028-1038.

[30] E.J.M. Hensen, Q. Zhu, R.A.J. Janssen, P. Magusin, P.J. Kooyman, R.A. van Santen, J. Catal. 233 (2005) 123-135.
[31] M.S. Kumar, M. Schwidder, W. Grunert, A. Bruckner, J. Catal. 227 (2004) 384-397.
[32] Y. Li, Z.C. Feng, H.C. Xin, F.T. Fan, J. Zhang, P. Magusin, E.J.M. Hensen, R.A. van Santen, Q.H. Yang, C. Li, J. Phys. Chem. B. 110 (2006) 26114-26121.
[33] S. Maurelli, M. Vishnuvarthan, M. Chiesa, G. Berlier, S. Van Doorslaer, J. Am. Chem. Soc. 133 (2011) 7340-7343.
[34] M. Strauss, G.A.V. Martins, G. Berlier, S. Coluccia, L. Marchese, H.O. Pastore, Micropor. Mesopor. Mat. 187 (2014) 135-144.
[35] M. Vishnuvarthan, V. Murugesan, E. Gianotti, L. Bertinetti, S. Coluccia, G. Berlier, Micropor. Mesopor. Mat. 123 (2009) 91-99.
[36] M. Vishnuvarthan, A.J. Paterson, R. Raja, A. Piovano, F. Bonino, E. Gianotti, G. Berlier, Micropor. Mesopor. Mat. 138 (2011) 167-175.
[37] A. Budnyk, A. Damin, E. Groppo, A. Zecchina, S. Bordiga, J. Catal. 324 (2015) 79-87.
[38] B. Ipek, R.F. Lobo, Chem. Commun. 52 (2016) 13401-13404.
[39] E.I. Solomon, Inorg. Chem. 45 (2006) 8012-8025.
[40] M.H. Groothaert, K. Lievens, J.A. van Bokhoven, A.A. Battiston, B.M. Weckhuysen, K. Pierloot, R.A. Schoonheydt, Chem. Phys. Chem. 4 (2003) 626-630.
[41] P.J. Smeets, R.G. Hadt, J.S. Woertink, P. Vanelderen, R.A. Schoonheydt, B.F. Sels, E.I. Solomon, J. Am. Chem. Soc. 132 (2010) 14736-14738.
[42] J.S. Woertink, P.J. Smeets, M.H. Groothaert, M.A. Vance, B.F. Sels, R.A. Schoonheydt, E.I. Solomon, P. Natl. Acad. Sci. USA. 106 (2009) 18908-18913.
[43] P. Vanelderen, B.E.R. Snyder, M.L. Tsai, R.G. Hadt, J. Vancauwenbergh, O. Coussens, R.A. Schoonheydt, B.F. Sels, E.I. Solomon, J. Am. Chem. Soc. 137 (2015) 6383-6392.
[44] B.M. Weckhuysen, in: B.M. Weckhuysen (Ed.), In-situ Spectroscopy of Catalysts, American Scientific Publishers, Utrecht University, The Netherlands, 2004, pp. 255-270.
[45] S.J. Tinnemans, J.G. Mesu, K. Kervinen, T. Visser, T.A. Nijhuis, A.M. Beale, D.E. Keller, A.M.J. van der Eerden, B.M. Weckhuysen, Catal. Today. 113 (2006) 3-15.
[46] P.D. Srinivasan, S.R. Nitz, K.J. Stephens, E. Atchison, J.J. Bravo-Suarez, Appl. Catal. A-Gen. 561 (2018) 7-18.
[47] M.H. Groothaert, P.J. Smeets, B.F. Sels, P.A. Jacobs, R.A. Schoonheydt, J. Am. Chem. Soc. 127 (2005) 1394-1395.
[48] E.I. Solomon, J.W. Ginsbach, D.E. Heppner, M.T. Kieber-Emmons, C.H. Kjaergaard, P.J. Smeets, L. Tian, J.S. Woertink, Faraday Discuss. 148 (2011) 11-39.
[49] E.I. Solomon, D.E. Heppner, E.M. Johnston, J.W. Ginsbach, J. Cirera, M. Qayyum, M.T. Kieber-Emmons, C.H. Kjaergaard, R.G. Hadt, L. Tian, Chem. Rev. 114 (2014) 3659-3853.
[50] F.C. Jentoft, Adv Catal. 52 (2009) 129-211.
[51] F.C. Meunier, React. Chem. Eng. 1 (2016) 134-141.
[52] J. Sirita, S. Phanichphant, F.C. Meunier, Anal. Chem. 79 (2007) 3912-3918.
[53] J.M. Olinger, P.R. Griffiths, Anal. Chem. 60 (1988) 2427-2435.
[54] A. Budnyk, A. Damin, C. Barzan, E. Groppo, C. Lamberti, S. Bordiga, A. Zecchina, J. Catal. 308 (2013) 319-327.
[55] M. Takeuchi, L. Bertinetti, G. Martra, S. Coluccia, M. Anpo, Appl. Catal. A-Gen. 307 (2006) 13-20.
[56] C.K. Jørgensen, in: F.A. Cotton (Ed.), Progress in Inorganic Chemistry, John Wiley & Sons, Hoboken, NJ, USA, 2007.
[57] P. Vanelderen, R.G. Hadt, P.J. Smeets, E.I. Solomon, R.A. Schoonheydt, B.F. Sels, J. Catal. 284 (2011) 157-164.
[58] V.L. Sushkevich, J.A. van Bokhoven, Chem. Commun. 54 (2018) 7447-7450.
[59] E. Borfecchia, P. Beato, S. Svelle, U. Olsbye, C. Lamberti, S. Bordiga, Chem. Soc. Rev. 47 (2018) 8097-8133.
[60] S.C. Larsen, A. Aylor, A.T. Bell, J.A. Reimer, J. Phys. Chem. 98 (1994) 11533-11540.
[61] J. Dedecek, B. Wichterlova, J. Phys. Chem.-Us. 98 (1994) 5721-5727.
[62] J. Dedecek, B. Wichterlova, P. Kubat, Micropor. Mesopor .Mat. 32 (1999) 63-74.
[63] H.J. Chen, M. Matsuoka, J.L. Zhang, M. Anpo, J. Catal. 228 (2004) 75-79.
[64] Q. Zhang, G.R. Chen, G.P. Dong, G. Zhang, X.F. Liu, J.R. Qiu, Q.L. Zhou, Q.X. Chen, D.P. Chen, Chem. Phys. Lett. 482 (2009) 228-233.

[65] P.-P.D.V. Knops-Gerrits, D. E.; Feijen, E. J. P.; Jacobs, P. A. , Microporous Materials. 8 (1997) 3-17.
[66] P. Chen, D.E. Root, C. Campochiaro, K. Fujisawa, E.I. Solomon, J. Am. Chem. Soc. 125 (2003) 466-474.
[67] D. Maiti, H.C. Fry, J.S. Woertink, M.A. Vance, E.I. Solomon, K.D. Karlin, J. Am. Chem. Soc. 129 (2007) 264-265.